NATO Science for Peace and Security Series - B:
Physics and Biophysics

Fundamental and Applied Nano-Electromagnetics

Edited by
Antonio Maffucci
Sergey A. Maksimenko

Springer

NATO OTAN

This publication is supported by:

The NATO Science for Peace and Security Programme

Chapter 5
Wave Packet Dynamical Calculations for Carbon Nanostructures

Géza I. Márk, Péter Vancsó, László P. Biró, Dmitry G. Kvashnin, Leonid A. Chernozatonskii, Andrey Chaves, Khamdam Yu. Rakhimov, and Philippe Lambin

Abstract Wave packet dynamics is an efficient method of computational quantum mechanics. Understanding the dynamics of electrons in nanostructures is important in both interpreting measurements on the nano-scale and for designing nanoelectronics devices. The time dependent dynamics is available through the solution of the time dependent Schrödinger- or Dirac equation. The energy dependent dynamics can be calculated by the application of the time-energy Fourier transform. We performed such calculations for various sp^2 carbon nanosystems, e.g. graphene grain boundaries and nanotube networks. We identified the global- and local structural properties of the system which influence the transport properties, such as the structures, sizes, and relative angles of the translation periodic parts, and the microstructure of the interfaces between them. Utilizing modified dispersion relations makes it possible to extend the method to graphene like materials as well.

Keywords Graphene • Wave packet dynamics • Quantum tunneling

G.I. Márk (✉) • P. Vancsó • L.P. Biró
Institute of Technical Physics and Materials Science, Centre for Energy Research, PO Box 49, H-1525 Budapest, Hungary
e-mail: mark@mfa.kfki.hu; http://www.nanotechnology.hu

D.G. Kvashnin • L.A. Chernozatonskii
Emanuel Institute of Biochemical Physics, 4 Kosigina Street, Moscow 119334, Russia

A. Chaves
Departamento de Física, Universidade Federal do Ceará, CP 6030, CEP 60455-900 Fortaleza, CE, Brazil

Kh.Yu. Rakhimov • P. Lambin
Department of Physics, University of Namur, rue de Bruxelles 61, 5000 Namur, Belgium

A. Maffucci, S.A. Maksimenko (eds.), *Fundamental and Applied Nano-Electromagnetics*, NATO Science for Peace and Security Series B: Physics and Biophysics, DOI 10.1007/978-94-017-7478-9_5

5.1 Introduction

Erwin Schrödinger introduced the concept of wave packets (WPs) in 1926 to bridge the gap between classical and quantum mechanics. The wave packet dynamical (WPD) method [1, 2] is a scattering experiment inside the computer: an incoming WP is "shot" into the localized potential representing the physical system and the time development of the WP is calculated by solving the time dependent Schrödinger (or Dirac) equation. Such carbon nanostructures as nanotube junctions, graphene grain boundaries, and scattering centers (electron-hole puddles) in graphene are generally too complex for conventional theoretical methods (e.g. DFT) – only small idealized models are tractable. WPD, however, is capable of calculating for realistic models containing several hundred atoms. Because of its dynamical nature, it is also possible to calculate electronic transport. This is indeed important in modeling the Scanning Tunneling Microscopy (STM) imaging and Scanning Tunneling Spectroscopy (STS) of carbon nanostructures, because the topography and the electronic structure information both influence the STM and STS results.

We performed WPD calculations for four different approximations with increasing accuracy: (i) jellium background model with Schrödinger equation; (ii) jellium model with Dirac equation; (iii) atomic pseudopotential model with Schrödinger equation; and (iv) multidomain method with Schrödinger equation, we will present all these models with characteristic applications in this paper.

5.2 Jellium Model Calculations with Schrödinger Equation

In this model the tunneling of an electron from the tip of the STM to the sample is regarded as a problem in potential scattering theory [3]. The time development of the $\psi\left(\vec{r},t\right)$ wave function is computed from the time dependent 3D Schrödinger equation using the split operator Fourier-transform method [4]

$$\psi\left(\vec{r},t+\Delta t\right)=e^{-i\widehat{H}\Delta t}\psi\left(\vec{r},t\right)$$

$$e^{-i\left(\widehat{K}+\widehat{V}\right)\Delta t}=e^{-i\widehat{K}\Delta t/2}e^{-i\widehat{V}\Delta t}e^{-i\widehat{K}\Delta t/2}+O\left(\Delta t^3\right)$$

where the potential energy propagator is a simple multiplication with $\exp\left(-iV\left(\vec{r}\right)\Delta t\right)$ for local potentials, and the effect of the kinetic energy propagator $\exp\left(-i\widehat{K}/2\Delta t\right)$ is given in k space by multiplicating the momentum space wave function by $\exp\left(-i\left|\vec{k}\right|^2\Delta t/4\right)$. The input parameters of the WPD method are the potential $V\left(\vec{r}\right)$ of the system and the $\psi\left(\vec{r},t_0\right)$ initial wave packet. From the calculated $\psi\left(\vec{r},t\right)$ wave function (output) we are able to obtain all

measurable quantities, such as the probability density $\rho(\vec{r},t)$, the probability current $\vec{j}(\vec{r},t)$, etc. One of the advantages of the split operator method is the norm conservation of the WP, which is necessary to calculate accurate transport values during the simulation time.

As we mentioned the tunneling phenomenon is determined by both the geometry and the electronic structure of the system. In order to understand the influence of these factors in the case of the STM – graphene system, first we focused on pure geometrical effects within the jellium potential model. Formerly we performed a detailed analysis of quantum effects arising purely from the geometry of the system which influence the STM imaging process of carbon nanotubes [5, 6]. Time dependent scattering of electronic WPs was calculated on a jellium potential model of the STM junction containing different arrangements of carbon nanotubes and point contacts. The theory allowed us to identify components of pure geometrical origin responsible for characteristic distortions of the STM image of carbon nanotubes. These geometrical effects can be well described within the framework of the jellium potential model. Recently we studied similar geometrical effects [7] in the STM imaging mechanism of a graphene sheet. The STM tip – graphene system has two important ingredients: an atomically sharp STM tip and a one atom thick graphene sheet. Figure 5.1a shows the vertical (xz) cross section of the model potential (z is the direction perpendicular to the graphene sheet). Within the framework of the jellium potential description of the STM tip – graphene nanosystem the STM tip is approached by a rotational hyperboloid of 0.5 nm apex radius and 15° aperture angle. The jellium potential value is zero outside the effective surface of the tip and −9.81 eV inside. This value was calculated from the HOPG EF = 5 eV Fermi energy and W = 4.81 eV work function. In first approximation the graphene sheet is taken as a jellium sheet of finite thickness, the potential inside the sheet is also set to −9.81 eV.

Figure 5.1b, c show the time evolution of the probability density of the WP. Figure 5.1b is a snapshot for $t = 1.95$ fs time, Fig. 5.1c is for $t = 3.61$ fs. This two particular time instants were chosen in the moment when the WP already started to tunnel from the tip apex into the sample ($t = 1.95$ fs) and when the WP is already spreading ($t = 3.61$ fs) on the jellium sheet. Majority of the WP is reflected back from the boundary of the tip potential into the tip; note the interference patterns inside the tip. After tunneling into the sheet, the WP cannot propagate further in the $-z$ direction of the incoming WP because of the large positive potential step at the lower boundary of the sheet. The WP is thus first accumulated in the jellium sheet below the tip apex and then it begins to spread along the sheet preserving its initial cylindrical symmetry. This is because the initial WP is not able to propagate along the z axis; its momentum has to be changed during the transient process from the vertical (z) into the horizontal (xy) direction. A transient period of length $\Delta t \approx 4$ fs can be defined while the probability current still flows between the tip and the surface. The jellium potential has a finite thickness of 0.09 nm and a −9.81 eV depth. The corresponding 1D potential well has a bound state at E = −3.1 eV. The tunneling event proceeds in two steps. First the WP tunnels into the bound

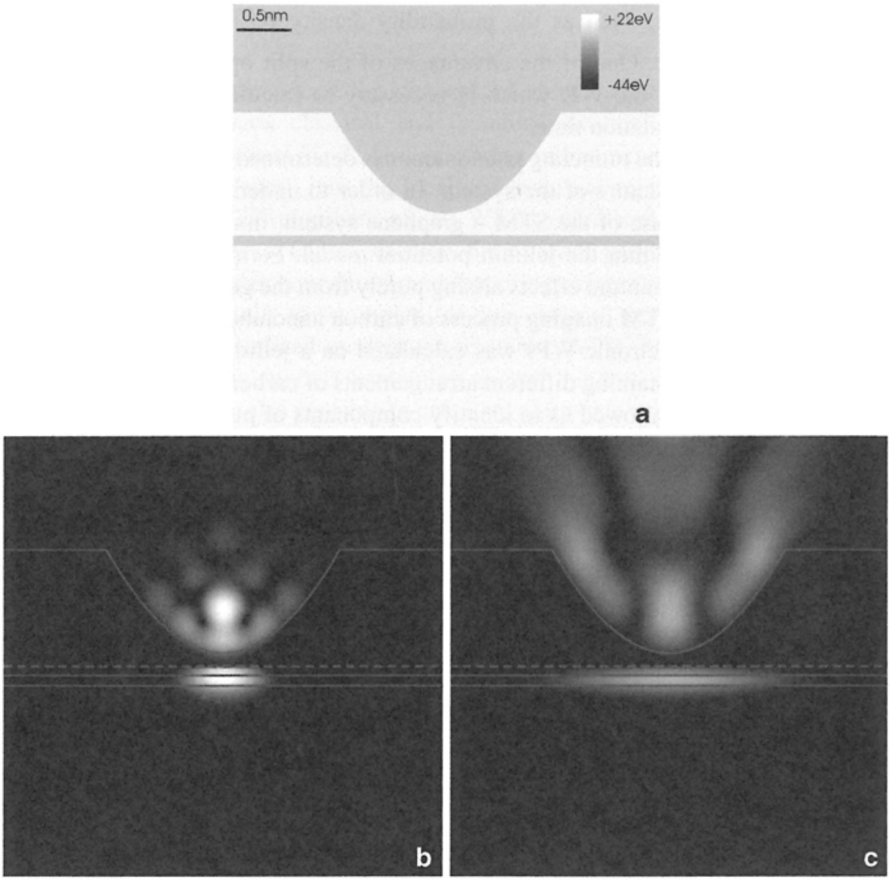

Fig. 5.1 Jellium model calculation for the STM tip—graphene system. (**a**) *Grayscale* image of the vertical (*xz*) cross section of the potential. The hyperbolic protrusion on the upper half plane and the thin gray horizontal bar represent the vertical cross sections of the tip and graphene, respectively. The *dark gray* level is the negative potential inside the STM tip and the jellium sheet (−9.81 eV), the *light gray* level is the vacuum potential (zero). The grayscale and the scalebar are chosen to match the minimum and maximum potential values of the graphene pseudopotential shown on Fig. 5.3a (see the text for details). (**b**) and (**c**) Selected snapshots from the time evolution of the probability density of wave packet shown as grayscale coded 2D sections. (**b**) $t = 1.95$ fs (c) $t = 3.61$ fs. *Black* corresponds to zero probability. The horizontal *dashed line* shows the position of the plane, where the tip-sample current was measured. We used a separate grayscale in the tip region and the sample region (above and below the *dashed line*) because the probability density in the sample is several orders of magnitude smaller than in the tip. The edges of the jellium electrodes are shown by *thin lines*

state of the jellium sheet. Then this quasi bound state begins to spread along the sheet. A selection process seems to operate during the transient period in the case of the narrow jellium plane, which means that after the transient process certain components of the WP are found to be tunneled back to STM tip and certain components are found to have remained on the jellium sheet.

5.3 Jellium Model Calculations with Dirac Equation

After discussing the geometrical effects we focus on the special electronic structure of graphene. Graphene, a single layer of graphite, is made out of carbon atoms arranged on a honeycomb lattice. This material has unique electronic properties due to the fact that the charge carriers in graphene follow linear dispersion relations [8] near the Fermi level, as if they were governed by the Dirac equation. The resulting massless Dirac-like quasiparticles give rise to peculiar quantum properties such as the Zitterbewegung [9]. In this section we have investigated the non-stationary Dirac equation for massless fermion in two dimensions which applies to low energy excitations in graphene [10]

$$-\frac{i}{\hbar}\frac{\partial}{\partial t}\Psi(x,y,t) = [v_F(\boldsymbol{\sigma}\boldsymbol{p}) + V(x,y)\,\mathbf{I}]\,\Psi(x,y,t),$$

where σ is the Pauli vector, I is the 2x2 identity matrix and the wave functions are written as pseudo-spinors $\Psi = \left(\Psi_A\ \Psi_B\right)^T$, where Ψ_A (Ψ_B) is the probability of finding the electron in the sub-lattice A (B) of graphene. We separate the potential and kinetic energy terms of the time-evolution operator through the split-operator technique [11]:

$$exp\left[-\frac{i}{\hbar}H\Delta t\right] = exp\left[-\frac{i}{2\hbar}V(x,y)\,\mathbf{I}\Delta t\right] exp\left[-\frac{i}{\hbar}v_F\mathbf{p}\cdot\boldsymbol{\sigma}\Delta t\right]$$
$$exp\left[-\frac{i}{2\hbar}V(x,y)\,\mathbf{I}\Delta t\right]$$

We have applied this formalism to the problem of puddles in graphene, which are regions rich in electrons or rich in holes, as observed experimentally [12, 13], due to the inevitable disorder in the graphene sheet. It is interesting to understand how such a disorder affects the reflection of electrons through graphene. At this aim, we have investigated recently [14] the WP propagation in graphene in the presence of randomly distributed circular potential steps. We assume that such a set of potentials might mimic the existence of electron and hole puddles in a real graphene sample, where these puddles appear with equal probability for electrons and holes [12]. Therefore, we assumed scattering centers that alternate between positive ($+V_0$) and negative ($-V_0$) potentials, considering that, locally, the electrons (holes) density is higher in negative (positive) potential regions, but the overall average potential in the whole scattering region is zero. This potential landscape is illustrated by the color maps in Fig. 5.2a, b for the two cases we have investigated in this work: S_1 (S_2) where 20 scattering centers of radius R = 5 nm (R = 7 nm) were considered, the width of the scattering zone being 40 nm (80 nm). Defining the density of scattering centers as $D_s = N_s\ \pi\ R^2/A$, where N_s is the number of circular scattering centers, and A is the area of the scattering region, one obtains $D_s = 0.303$ for both cases. By comparing S_1 to S_2, we intend to analyze the combined effect of width of the

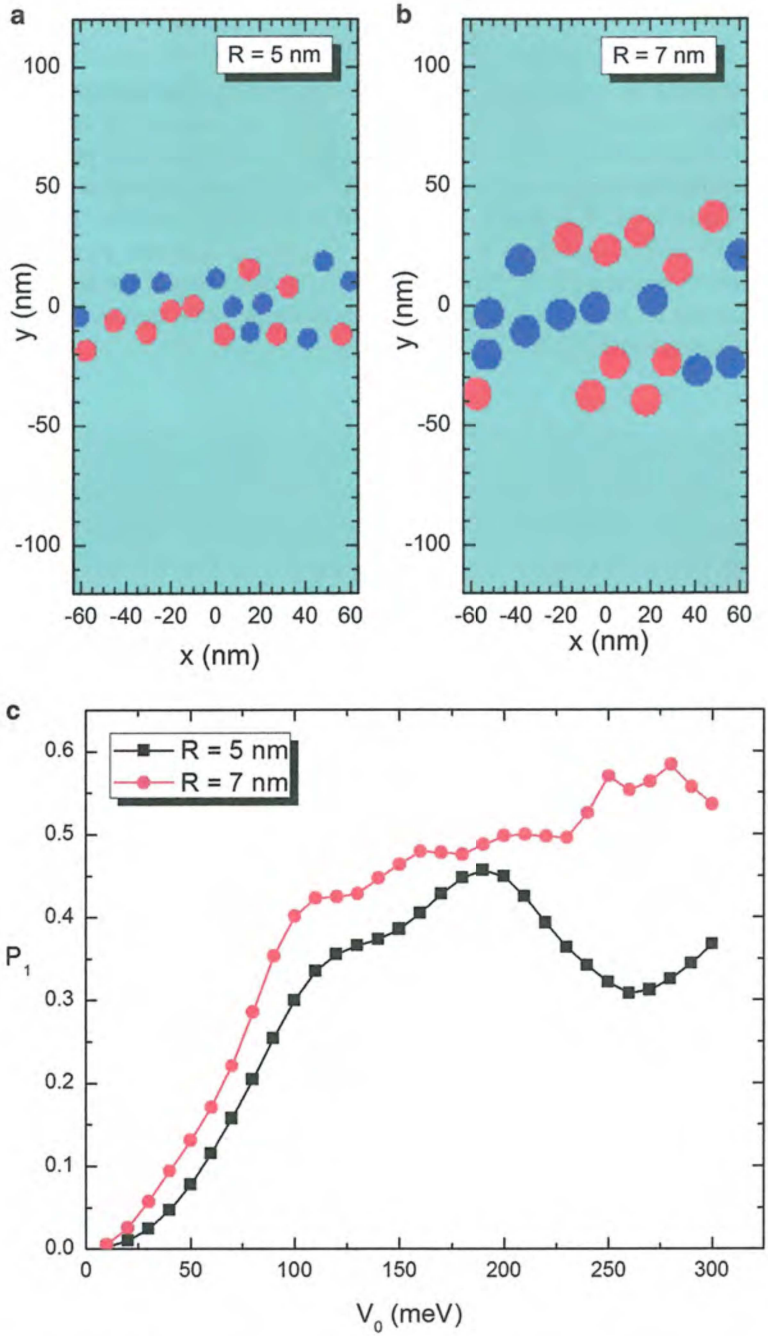

Fig. 5.2 (**a**) and (**b**) Color map of the random potential landscape for the two sample cases considered in this section: S1 and S2 with 20 dots of radius R = 5 nm and R = 7 nm, respectively. (**c**) The reflectance of the barrier, computed as the largest limit of backscattering probability, is illustrated versus potential barrier V_0 for the two sample cases S_1 and S_2

scattering region and the radius of the puddles, since S_2 is twice wider than S_1 but it has the same density D_s. All the results presented in this section were obtained for a wave packet with average energy E = 100 meV and $a_y = 20$ nm. The WP had an infinite size in x.

From the numerical solution of the Dirac-Weyl equation the probability current density was computed from which reflection and transmission probabilities were derived. Figure 5.2c shows the saturation value of the reflection probability P_1 as a function of the potential barrier V_0, for the two sample cases considered in this work. In both cases, the reflection probabilities monotonically increase with increasing potential height until $V_0 = 100$ meV, where the Klein tunneling of non-normal incident parts of the WP is minimal, since this value of V_0 is close to the WP energy E = 100 meV [15, 16]. Above this value, the reflection probabilities oscillate from 0.3 to 0.6. The reflection probability is larger for the stronger perturbation (S_2) among the two cases examined here.

5.4 Local Pseudopotential Calculations with Schrödinger Equation

Dirac equation methods nicely describe the electronic dynamics in graphene near the Fermi level, where the dispersion relation is linear. Away from the Fermi level, however, the dispersion relation is not any more linear (and not any more isotropic), hence we need another method to describe high (and low) energy dynamics of the π band correctly. This was accomplished by utilizing an atomic pseudopotential [17] matching the band structure of the graphene sheet π electrons. The π electron approximation is valid as long as the structure remains flat. Moreover the atomistic approach makes us possible to handle local effects, such as grain boundaries in graphene. This local one electron potential has the following form

$$V_{graphene}\left(\vec{r}\right) = \sum_{j=1}^{N} \sum_{i=1}^{3} A_i e^{-a_i \left|\vec{r} - \vec{r}_j\right|^2},$$

where $\vec{r}_j$ denote the atomic positions and N is the number of atoms. The A_i, a_i coefficients are given in reference [17]. Figure 5.3a shows the vertical (xz) cross section of the model potential.

Details of the time evolution of the WP on the graphene surface (xy cross section) can be seen in Fig. 5.3b, c. As the WP reaches the tip apex from inside the tip bulk, it begins to tunnel onto the central hexagon. Then the WP begins to spread on the graphene sheet along the C-C bonds, in hexagonal symmetry (cf. Fig. 5.3b). In this atomic scale process the WP does not "notice" the infinite hexagonal lattice, only follows the pattern of the pseudopotential which has low value channels between the nearest neighbour C-C bonds, and positive values at the centres of the

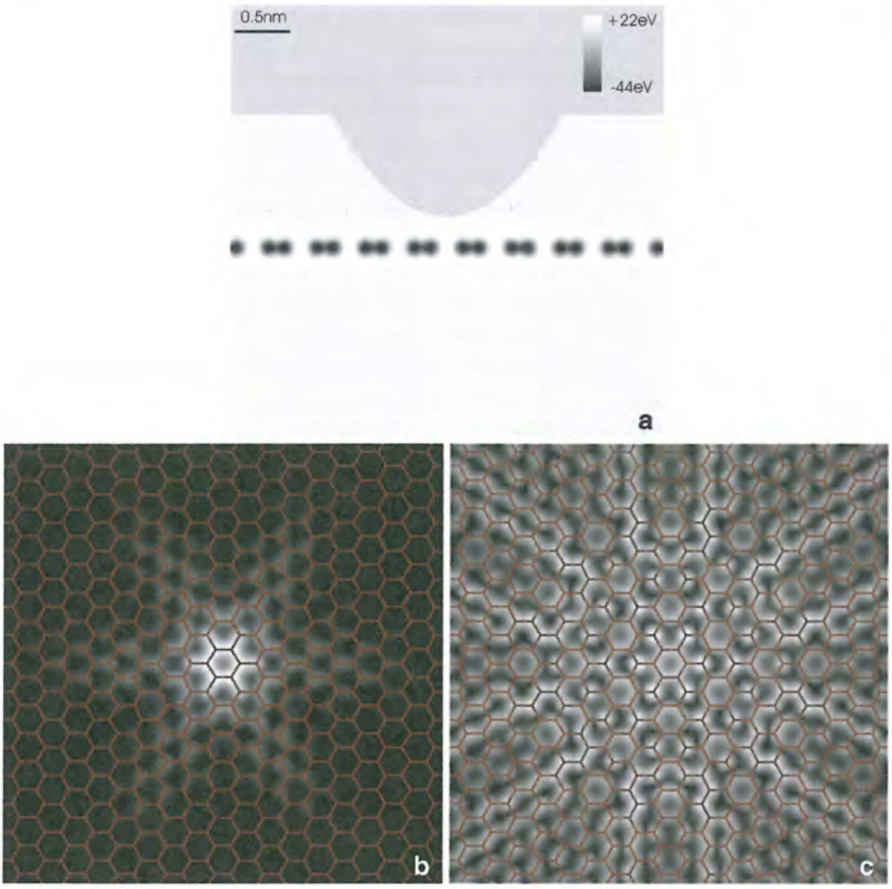

Fig. 5.3 Atomic pseudopotential calculations for a quasiparticle tunneling from the STM tip onto the graphene sheet. The STM tip is above the center of a hexagon. (**a**) Grayscale image of the vertical (*xz*) cross section of the local one electron potential. (**b**) and (**c**) Selected snapshots ($t = 2.71$ fs and 4.29 fs) from the time evolution of the probability density of the wave packet on the graphene sheet shown as grayscale coded 2D sections (at the *xy* plane). Black corresponds to zero probability, white is the maximum probability. Each image is separately normalized. The graphene network is shown by thin orange lines

hexagons. This stage can be regarded as a "molecular" spreading. The direction of the spreading has changed at t = 3.14 fs. The new propagation direction is (cf. Fig. 5.3c) matching the zigzag direction of the graphene sheet in direct space which is equivalent to the 6 ΓK directions of the Brillouin-zone – thus the WP begins to "feel" the infinite hexagonal lattice, hence this stage can be regarded as a "solid state" spreading in which the preferential directions are determined by the lattice symmetry [18].

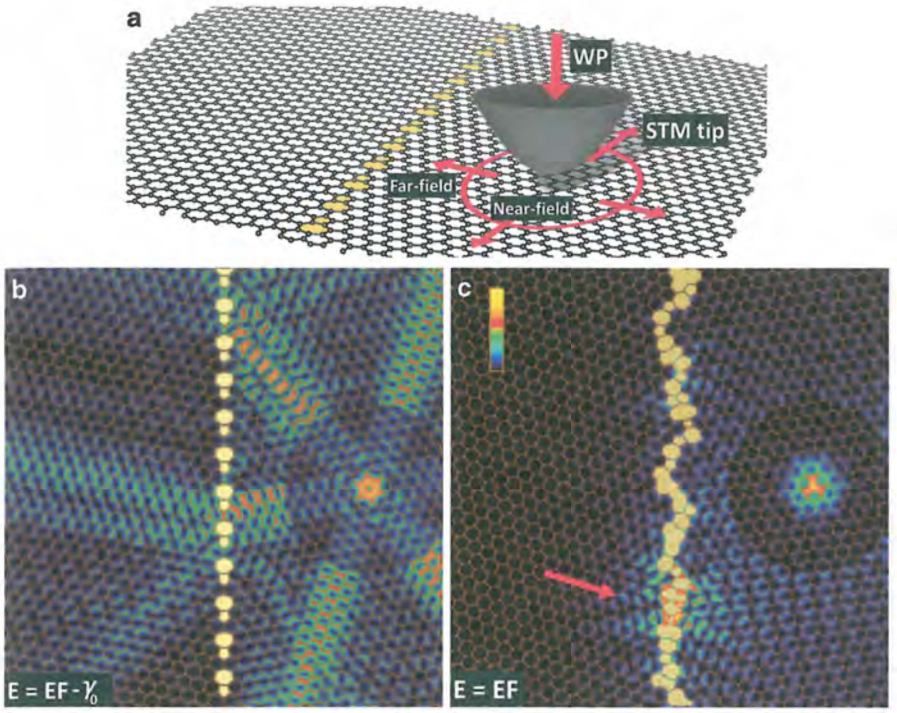

Fig. 5.4 Charge transfer through a graphene grain boundary. (**a**) Model geometry of the STM tip – graphene system for the case of the pentagon-heptagon grain boundary. STM tip modeled with a rotational hyperboloid of jellium is presented by the −2.7 eV equipotential surface of the potential. *Red arrows* symbolize the incoming and spreading directions of the wave packet. Below the STM tip the *red circle* denotes the near-field region, where the STM tip has strong influence on the wave functions. (**b**) Probability density on the graphene sheet with the 5–7 grain boundary for $E = -\gamma_0$ as a colour coded 2D (XY) section. Different colour scales were used in the near- and far regions (inside and outside of the circle). The GB works as a beam-splitter for the electrons spreading anisotropically along the zig-zag directions. (**c**) Probability density on the graphene sheet with a disordered grain boundary around the Fermi energy as a color coded 2D (XY) section. Note the strong localization around a four membered carbon ring, denoted by a *red arrow*

We successfully applied the atomic pseudopotential method for a number of carbon nanosystems of practical importance. Figures 5.4 and 5.5 shows two examples, for a graphene grain boundary and for a hexagonal network of nanotubes (a superlattice). In order to study the dynamics in the energy, we used a time-energy ($t \rightarrow E$) Fourier transform, thus obtaining the energy dependent wave function $\psi\left(\vec{r}, E\right)$ from the time dependent wave function $\psi\left(\vec{r}, t\right)$ (which is the output of the WPD calculation).

Figure 5.4 shows the wave packet transport through an ordered and through a disordered graphene grain boundary. As shown by AFM measurements [19], a real graphene sheet breaks into many single-crystal regions between the domains and

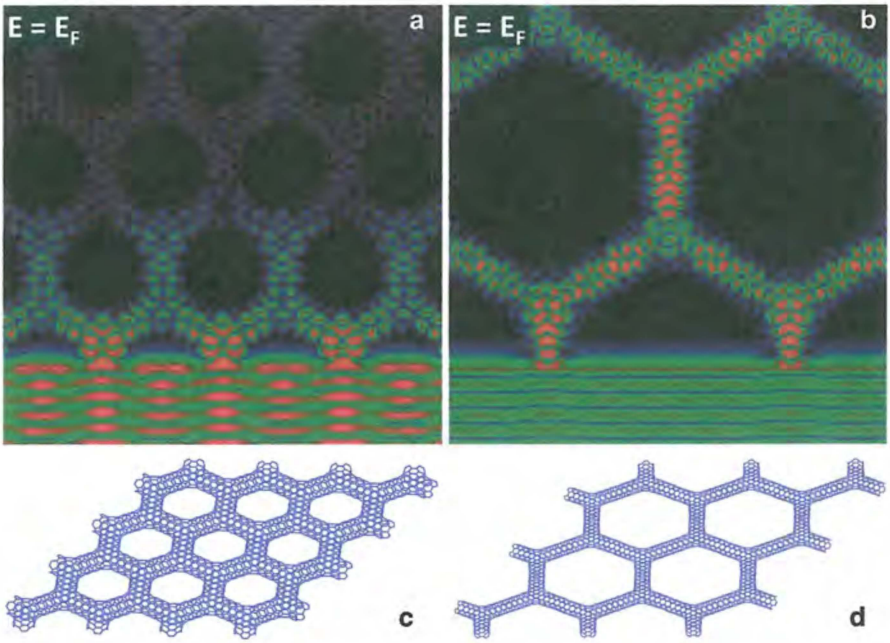

Fig. 5.5 (**a**) and (**b**) Wave packet dynamics calculated probability densities for bilayered graphene structures at the Fermi energy. (**a**) A semiconductor structure – the wave packet does not penetrate the lattice. (**b**) A metallic structure – the wave packet travels through the lattice. (**c**) and (**d**) Model geometries for the semiconducting (**a**) (metallic (**b**)) case, respectively

the presence of the grain boundaries substantially affect the remarkable properties of the perfect graphene [20]. The transport properties of the grain boundaries can be significantly different depending on their detailed geometry, as shown on Fig. 5.4. Figure 5.4a shows the geometry of the calculation. The simulated STM tip is placed above the right hand side grain and the WP is injected into this grain. Figure 5.4b, c show the probability density of the wave packet for an ordered and for a disordered grain boundary, respectively. Figure 5.4b is for $E = E_F\text{-}\gamma_0$, where $\gamma_0 = 2.7$ eV is the tight-binding first neighbor integral. At this energy the charge propagation is highly anisotropic. This so called "trigonal warping" phenomenon is not described by the Dirac equation model of graphene. Our detailed investigations [21–23] showed a reduced transport for the disordered grain boundaries, primarily attributed to electronic localized states caused by C atoms with only two covalent bonds.

Figure 5.5 shows results of a wave packet dynamical calculation for nanomeshes based on bilayered graphene. Our large scale *ab-initio* calculations showed [24] that fabrication of hexagonal holes in bigraphene leads to connection of the neighboring edges of the two graphene layers with formation of a hollow carbon nanostructure sheet which displays wide range of electronic properties (from semiconductor to metallic), depending on the size of the holes and the distance between them.

Our WPD calculations shown on Fig. 5.5. further supported this result. Indeed, no conducting state (only an evanescent state) is seen on the Fermi energy for a semiconductor nanomesh, while we see a conducting state on the Fermi energy for the metallic nanomesh.

5.5 Multidomain Wave Packet Dynamical Calculations

As we explained earlier, the split operator method approximates the exact time development by three consecutive operations in each time step: a pure kinetic energy propagation for $\Delta t/2$, a pure potential energy propagation for Δt, and a final pure kinetic energy propagation for $\Delta t/2$. The kinetic energy propagation is calculated in Fourier space, i.e. the momentum space wave function $\psi(\vec{k}, t)$ is multiplied by the $\exp\left(-i|\vec{k}|^2 \Delta t/4\right)$ free space propagator. Indeed, for a potential free ($V = 0$) propagation, the dispersion relation is $E \propto |\vec{k}|^2$ and the split time approximation provides the exact result for this case. This technique makes it easy to replace the free space parabolic dispersion relation by any $E = E(\vec{k})$ function. Figure 5.6 shows the time development of the WP for a parabolic (Fig. 5.6a) and a linear (Fig. 5.6b) dispersion relation. The WP propagating with parabolic dispersion relation shows the usual spreading phenomenon: the width of the WP is increasing and the height of the WP is decreasing simultaneously – note the decreasing density values for larger times. The WP propagating with linear dispersion relation behaves differently: no spreading is seen. The shape (width and height) remains unchanged during the time development, only the location of the WP is changing during the propagation. This is similar to the propagation of an electromagnetic wave impulse in a dispersionless medium. Figure 5.6c shows a multidomain propagation, the dispersion relation is parabolic on the left side and linear on the right side, with a gradual interface region between them, to prevent reflection. Note the presence of spreading on the left side and the absence of spreading on the right side.

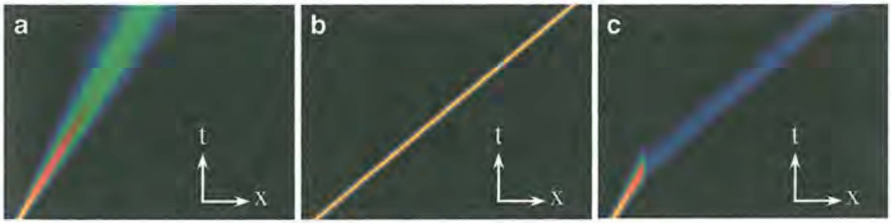

Fig. 5.6 Time development of a one dimensional wave packet shown as x-t spacetime density plots. (**a**) Parabolic dispersion relation. (**b**) Linear dispersion relation. (**c**) Two domains, *left* (*right*) domain with parabolic (*linear*) dispersion. *Black* corresponds to zero probability

5.6 Conclusions

We have presented a detailed analysis of different techniques of wave packet dynamical calculations for carbon nanostructures. Geometrical effects in Scanning Tunneling Microscopy, such as image distorsions seen in experimental images can be successfully explained [5] by utilizing a jellium potential model in the time dependent Schrödinger equation. The peculiar electronic structure of graphene – linear and isotropic dispersion relation near the Fermi energy – makes it possible to utilize the time dependent Dirac equation [14] in WPD. With this model we can study all electronic structure and transport phenomena involving low energy excitations only, as we demonstrated for the case of electron–hole puddles in graphene. In order to describe processes involving higher energy excitations, as well as defects, we developed a local one electron pseudopotential [17] matching the electronic structure of the whole Pi band of graphene. As we demonstrated with DFT [21] and tight-binding [23] calculations, this potential correctly describes all sp^2 carbon structures, such as in grain boundaries in graphene and bilayered graphene superlattices [24]. The construction of a local one-electron pseudopotential needs a tedious variational procedure [17], however, and it is even not possible for any materials. In order to extend the WPD method to other materials, we can, however, utilize that the split operator Fourier transform method computes the effect of the kinetic energy operator in momentum space. This makes it possible to change the free space parabolic dispersion relation with any $E = E\left(\vec{k}\right)$ function – as we demonstrated for simple one dimensional examples. This means that we can extend the WPD method to any material, where band structure calculations are available. By applying different dispersion relations in different spatial regions (domains), we can even model physical systems containing different materials. Such multidomain WPD calculations are underway for complex systems, such as transition metal dichalcogenide (TMDC) materials.

To conclude, wave packet dynamics is capable not only of explaining experimental results on carbon nanosystems, but it can also be useful in designing carbon nanoelectronic devices.

Acknowledgements This work was supported by an EU Marie Curie International Research Staff Exchange Scheme Fellowship within the 7th European Community Framework Programme (MC-IRSES proposal 318617 FAEMCAR project), Graphene Flagship (Graphene-Based Revolutions in ICT And Beyond, GRAPHENE, Grant agreement number 604391), and the OTKA 101599 in Hungary. We are grateful to the Joint Supercomputer Center of the Russian Academy of Sciences and "Lomonosov" research computing center for the possibilities of using a cluster computer for the quantum-chemical calculations. ACh acknowledges financial support from CNPq, through the PRONEX/FUNCAP and Science Without Borders programs. KhR is grateful to the University of Namur for funding. GIM acknowledges the support of the Belgian FNRS.

References

1. Garraway BM, Suominen K-A (1995) Wave-packet dynamics: new physics and chemistry in femto-time. Rep Prog Phys 58:365–419
2. Varga G (2002) Computer simulation by the quantum mechanical time-dependent wavepacket method, especially for atom/molecule-solid-surface interaction. J Phys Condens Matter 14:6081–6107
3. Lucas AA, Morawitz H, Henry GR, Vigneron J-P, Lambin P, Cutler PH, Feuchtwang TE (1988) Scattering-theoretic approach to elastic one-electron tunneling through localized barriers: application to scanning tunneling microscopy. Phys Rev B 37:10708–10720
4. Feit MD, Fleck JA, Steiger A (1982) Solution of the Schrödinger equation by a spectral method. J Comput Phys 47:412–433
5. Márk GI, Biró LP, Gyulai J (1998) Simulation of STM images of 3D surfaces and comparison with experimental data: carbon nanotubes. Phys Rev B 58:12645–12648
6. Márk GI, Biró LP, Lambin Ph (2004) Calculation of axial charge spreading in carbon nanotubes and nanotube Y-junctions during STM measurement. Phys Rev B 70, 115423-1-11
7. Vancsó P, Márk GI, Lambin P, Hwang C, Biró LP (2012) Time and energy dependent dynamics of the STM tip — graphene system. Eur Phys J B 85:142–149
8. Novoselov KS, Geim AK, Morozov SV, Jiang D, Katsnelson MI, Grigorieva IV, Dubonos SV, Firsov AA (2005) Two-dimensional gas of massless Dirac fermions in graphene. Nature 438:197–200
9. Cserti J, Dávid Gy (2006) Unified description of Zitterbewegung for spintronic, graphene, and superconducting systems. Phys Rev B 74, 172305-1-4
10. Castro AH, Guinea F, Peres NMR, Novoselov KS, Geim AK (2009) The electronic properties of graphene. Rev Mod Phys 81:109–162
11. Degani MH, Leburton JP (1991) Single-electron states and conductance in lateral-surface superlattices. Phys Rev B 44:10901–10904
12. Martin J, Akerman N, Ulbricht G, Lohmann T, Smet JH, von Klitzing K, Yacoby A (2008) Observation of electron–hole puddles in graphene using a scanning single-electron transistor. Nat Phys 4:144–148
13. Schubert G, Fehske H (2012) Metal-to-insulator transition and electron-hole puddle formation in disordered graphene nanoribbons. Phys Rev Lett 108 066402-1-5
14. Yu Kh, Rakhimov AC, Farias GA (2013) Low-dimensional functional materials. Egger R, Matrasulov D, Rakhimov Kh (eds). Springer, Dordrecht
15. Matulis A, Peeters FM (2008) Quasibound states of quantum dots in single and bilayer graphene. Phys Rev B 77, 115423-1-11
16. Yu Kh, Rakhimov A, Chaves G, Farias A, Peeters FM (2011) Wavepacket scattering of Dirac and Schrödinger particles on potential and magnetic barriers. A. J. Phys Condens Matter 23, 275801
17. Mayer A (2004) Band structure and transport properties of carbon nanotubes using a local pseudopotential and a transfer-matrix technique. Carbon 42:2057–2066
18. Márk GI, Vancsó P, Hwang C, Lambin Ph, Biró LP (2012) Anisotropic dynamics of charge carriers in graphene. Phys Rev B 85, 125443-1-12
19. Nemes-Incze P, Yoo KJ, Tapasztó L, Dobrik G, Lábár J, Horváth ZE, Hwang C, Biró LP (2011) Revealing the grain structure of graphene grown by chemical vapor deposition. Appl Phys Lett 99, 023104-1-3
20. Biró LP, Lambin Ph (2013) Grain boundaries in graphene grown by chemical vapor deposition. New J Phys 15, 035024-1-3
21. Nemes-Incze P, Vancsó P, Osváth Z, Márk GI, Jin X, Kim Y-S, Hwang C, Lambin P, Chapelier C, Biró LP (2013) Electronic states of disordered grain boundaries in graphene prepared by chemical vapor deposition. Carbon 64:178–186

22. Vancsó P, Márk GI, Lambin P, Mayer A, Kim Y-S, Hwang C, Biró LP (2013) Electronic transport through ordered and disordered graphene grain boundaries. Carbon 64:101–110
23. Vancsó P, Márk GI, Lambin P, Mayer A, Hwang C, Biró LP (2014) Effect of the disorder in graphene grain boundaries: a wave packet dynamics study. Appl Surf Sci 291:58–63
24. Kvashnin DG, Vancsó P, Yu L, Antipina, Márk GI, Biró LP, Sorokin PB, Chernozatonskii LA (2015) Bilayered semiconductor graphene nanostructures with periodically arranged hexagonal holes. Nano Res 8:1250–1258